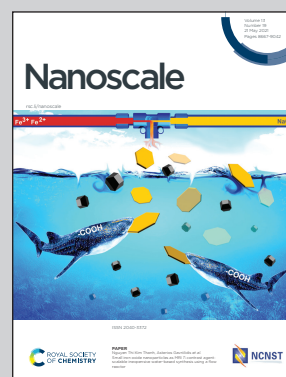Showcasing research from the Nanoscience Research Group (Department of Physics, Tokyo Metropolitan University).

Air-stable and efficient electron doping of monolayer MoS_2 by salt–crown ether treatment

Air-stable and highly efficient electron doping of monolayer MoS_2 has been achieved by crown ether complexes containing potassium ion.

ROYAL SOCIETY
OF **CHEMISTRY**

rsc.li/nanoscale

Air-stable and efficient electron doping of monolayer MoS$_2$ by salt–crown ether treatment†

Hiroto Ogura, [iD] [a] Masahiko Kaneda,[a] Yusuke Nakanishi, [iD] [a]
Yoshiyuki Nonoguchi, [iD] [b] Jiang Pu,[c] Mari Ohfuchi,[d] Toshifumi Irisawa,[e]
Hong En Lim, [iD] [a] Takahiko Endo,[a] Kazuhiro Yanagi,[a] Taishi Takenobu [iD] [c] and
Yasumitsu Miyata [iD] *[a]

To maximize the potential of transition-metal dichalcogenides (TMDCs) in device applications, the development of a sophisticated technique for stable and highly efficient carrier doping is critical. Here, we report the efficient n-type doping of monolayer MoS$_2$ using KOH/benzo-18-crown-6, resulting in a doped TMDC that is air-stable. MoS$_2$ field-effect transistors show an increase in on-current of three orders of magnitude and degenerate the n-type behaviour with high air-stability for ~1 month as the dopant concentration increases. Transport measurements indicate a high electron density of 3.4×10^{13} cm^{-2} and metallic-type temperature dependence for highly doped MoS$_2$. First-principles calculations support electron doping *via* surface charge transfer from the K/benzo-18-crown-6 complex to monolayer MoS$_2$. Patterned doping is demonstrated to improve the contact resistance in MoS$_2$-based devices.

Introduction

Two-dimensional (2D) transition-metal dichalcogenides (TMDCs) have attracted much attention because of their excellent physical properties and potential applications in electronics and optoelectronics.[1–7] In particular, much effort has recently been devoted to investigate group-6 TMDC monolayers such as MoS$_2$ and WSe$_2$ and to elucidate their semiconducting properties, such as high on/off current ratio, high mobility and direct-bandgap nature.[8–13] To exploit the potential of TMDCs in devices such as light-emitting diodes and tunnelling field-effect transistors (FETs), developing a sophisticated technique for stable and highly efficient carrier doping is critical.

Carrier doping in TMDCs has been carried out *via* several approaches, including elemental substitution, defect engineering, and chemical doping. Elemental substitution of group-6 TMDCs has been demonstrated by replacing group-6 transition metal elements (Mo and W) with group-5 and group-7 elements such as Nb and Re, respectively.[14–18] Defect engineering has been carried out by the formation of chalcogen vacancies by hydrazine or plasma treatment,[19,20] and the replacement of sulphur vacancies by chloride molecules.[21] Even though these techniques enable high tunability of the electrical conductivity of TMDCs, achieving both high-density doping and high mobility remains a major challenge because of impurity scattering by the substituted atoms or defects. In contrast, chemical doping is mainly based on surface charge transfer from a dopant to a semiconductor and has the advantage of not usually introducing defects into the crystal lattice. Chemical doping can thus increase the carrier density without seriously degrading the carrier mobility of TMDCs. The literature contains numerous reports of TMDC doping.[22–31] For example, Fang *et al.* reported degenerate n-type doping of few-layer MoS$_2$ and WSe$_2$ *via* vapor-phase doping of K, resulting in high electron densities of $\sim 1.0 \times 10^{13}$ cm^{-2} and $\sim 2.5 \times 10^{12}$ cm^{-2} for MoS$_2$ and WSe$_2$, respectively.[22] Air-stable n-type doping of few-layer MoS$_2$ with a high carrier density of $\sim 1.2 \times 10^{13}$ cm^{-2} was also achieved *via* solution-based doping of benzyl viologen (BV); the BV-doped MoS$_2$ exhibited stable transport properties in air for ~9 days.[23] Ji *et al.* achieved p- and n-type doping of monolayer WSe$_2$ using 4-nitrobenzene-diazonium tetrafluoroborate and diethylenetriamine, respectively, and reported high carrier mobilities of 82 and 25 cm^2 V^{-1} s^{-1} for holes and electrons, respectively.[29] Despite such progress, further improvements that result in highly stable and efficient doping methods are strongly desired for realizing future high-performance TMDC-based devices.

In the present work, we demonstrate the feasibility of using salt–crown ethers to achieve degenerate n-type, stable monolayer MoS$_2$. Crown ethers, which are cyclic oligomers consisting of several ethylene oxides, possess central cavities that form stable complexes with various metal ions and

[a]*Department of Physics, Tokyo Metropolitan University, Hachioji, 192-0397, Japan. E-mail: ymiyata@tmu.ac.jp*
[b]*Faculty of Materials Science and Engineering, Kyoto Institute of Technology, Kyoto 606-8585, Japan*
[c]*Department of Applied Physics, Nagoya University, Nagoya, 464-8603, Japan*
[d]*Fujitsu Laboratories Ltd, Atsugi, 243-0197, Japan*
[e]*Nanoelectronics Research Institute, AIST, Tsukuba, 305-8562, Japan*
†Electronic supplementary information (ESI) available. See DOI: 10.1039/d1nr01279g

molecules.[32,33] One type of crown ether, benzo-18-crown-6 in KOH/butanol solution, forms stable complexes with K^+ cations to produce OH^- anions, which can serve as an efficient n-type dopant for carbon nanotubes (CNTs).[32] We found that this approach is also effective at preparing highly doped monolayer MoS_2 with an electron density of 3.4×10^{13} cm^{-2}, which is similar to the previously reported electron density values for MoS_2 doped with other n-type dopants such as K and BV.[22,23] Importantly, the electron-doped surfaces of MoS_2 are stable under ambient conditions for approximately 1 month. The electron doping by the crown ether complex is also supported by the first principles calculations. Furthermore, patterned doping is demonstrated to improve the contact resistance in MoS_2-based FETs.

Results and discussion

To investigate the carrier doping by crown ether in MoS_2, back-gated FETs with a MoS_2 channel were fabricated. Fig. 1a shows

the schematic and optical micrographs of a representative MoS_2 FET. Triangular -shaped monolayer MoS_2 single crystals were grown on SiO_2/Si substrates via chemical vapor deposition (CVD). For n-type doping, the samples were spin-coated with a butanol solution of KOH/benzo-18-crown-6. In the solution, K^+ ions were captured by the cavities of the crown ether to form stable K^+-ion complexes $[K\text{-crown}]^+OH^-$ in butanol.[32]

$$KOH + [crown] \rightleftharpoons [K\text{-crown}]^+ + OH^-$$
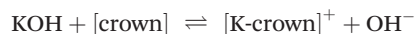
Similar to the case of CNTs, we reasonably expected electrons to transfer from OH^- ions to MoS_2; we also expected the transferred electrons to be stabilized by $[K\text{-crown}]^+$ cations adsorbed onto the MoS_2 surface, as illustrated in Fig. 1b. The positive charges in the metal ion–benzocrown complexes would be delocalized over the benzene ring, thereby supporting further stabilization of negatively charged K^+ ions.[32]

Fig. 1c and d presents the transfer and output curves for FETs with undoped MoS_2 and FETs with MoS_2 doped with KOH/benzo-18-crown-6 at concentrations from 0.1 to 100 mM, respectively. The undoped MoS_2 exhibits typical n-type
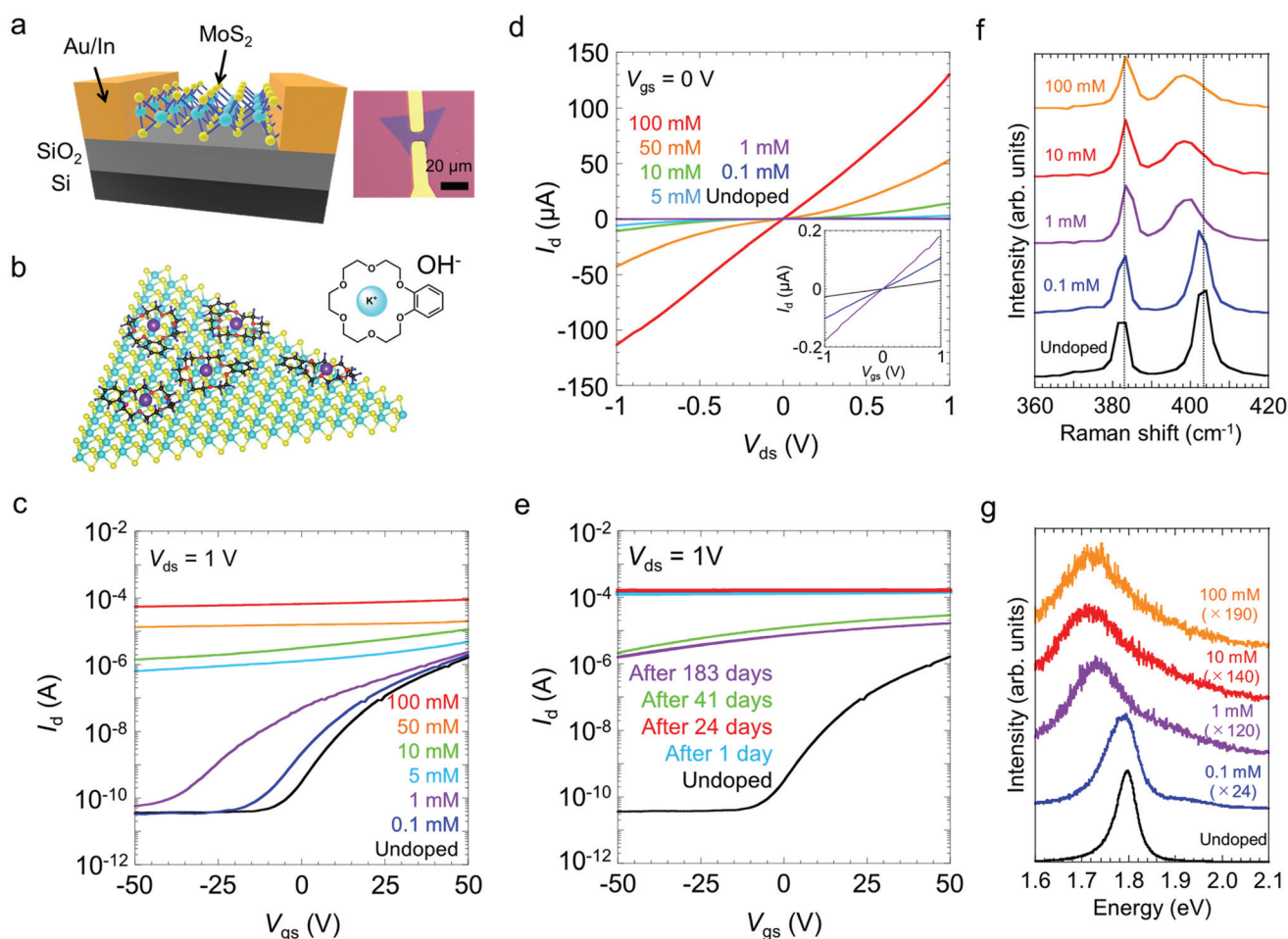

Fig. 1 (a) Schematic and optical micrographs of the back-gated FET device. (b) Schematic model of the chemical doping using KOH/benzo-18-crown-6 for n-type doping. (c and d) The transfer (c) and output curves (d) of undoped and doped monolayer MoS_2 with different dopant concentrations from 0.1 to 100 mM. (e) Transfer characteristic curves of the device before and after doping. The doped device had been kept in air for 183 days. (f and g) Raman (f) and PL (g) spectra of undoped and doped monolayer MoS_2 with different dopant concentrations from 0.1 to 100 mM.

semiconducting behaviour; the corresponding FET exhibits an on/off current ratio of ~10^5 and a carrier mobility of ~6.5 cm^2 V^{-1} s^{-1} for applied gate voltages, V_{gs}, ranging from −50 to 50 V. Here, the carrier mobility was estimated using a parallel-plate model,[34] $\mu = [(dI_d)/(dV_{gs})][(L/V_{ds}C_{OX}W)]$, where L is the channel length, W is the channel width, I_d is the drain current, V_{ds} is the drain voltage, and C_{OX} = 12.1 nF cm^{-2} is the gate capacitance of SiO$_2$ with a thickness of 285 nm and V_{ds} = 1 V. These characteristics are comparable to those reported in previous studies of CVD-grown monolayer MoS$_2$.[35] For the samples coated with 0.1 and 1 mM dopants, higher-concentration doping led to a shift of the threshold voltage (V_{th}) to the negative voltage side and to an increase of the drain current. Treatments with higher-concentration dopants resulted in a substantial increase in the off-current and in metallic gate dependence. Eventually, the on-current reached ~100 μA for the sample treated with the 100 mM dopant solution, which represents an increase of approximately two orders of magnitude compared with the on-current of the untreated sample. An increase in the on-current was also observed for monolayer WS$_2$ (Fig. S1†). Notably, the doped MoS$_2$ FETs were highly stable in ambient air. The transfer curves remained nearly unchanged even after 24 days of air exposure (Fig. 1e). The drain current decreased by one order of magnitude between 24 and 41 days, but showed little change for the next 142 days.

The doped MoS$_2$ was further characterized by Raman and photoluminescence (PL) spectroscopy. Fig. 1f shows the Raman spectra of monolayer MoS$_2$, recorded before and after the doping treatments with different concentrations of the dopants (0.1–100 mM). The two characteristic Raman peaks denoted by E′ and A′$_1$ are attributed to the in-plane and out-of-plane vibration modes of monolayer MoS$_2$, respectively.[36] As shown in Fig. 1f, the E′ mode (383 cm^{-1}) changes very little after the doping process, whereas the A′$_1$ mode is downshifted by 6 cm^{-1}. This tendency is consistent with the results of an earlier report of electron doping of MoS$_2$ with BV[23] and suggests that the electron–phonon interaction is enhanced by an increase in the electron concentration.[37] The PL spectra show the emission peak from A exciton at 1.80 eV for the undoped MoS$_2$ (Fig. 1g).[8] The A-exciton peak was substantially suppressed by the doping treatments and was completely quenched at above 1 mM with a downshift of the peak to 1.72 eV. Similar quenching of the A-exciton peak is also observed for the doping by electric field.[38] These PL changes can be explained by an increase of the emission from negatively charged trions as a result of the electron doping and the suppression of neutral exciton formation.[38,39] These optical responses are consistent with the transport measurement results for electron-doped monolayer MoS$_2$. A good homogeneity of doping was confirmed by the Raman and PL spectra obtained at different locations (Fig. S2†). A small variation in the PL spectra is also observed for both the pristine and doped samples and can be explained by the local lattice strain induced due to the interaction with the growth substrate.[40]

We measured the Hall effect and the temperature dependence of the electrical resistance of the sample doped using
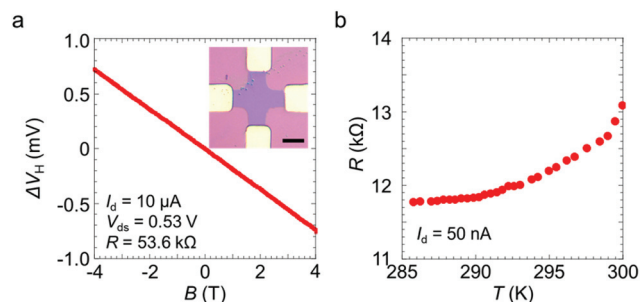

Fig. 2 (a) Magnetic field dependence of the Hall voltage for the doped monolayer MoS$_2$ using 100 mM dopant solution at room temperature. The inset is an optical image of the sample. The scale bar is 10 μm. (b) Temperature dependence of the electrical resistance for the doped monolayer MoS$_2$ using 100 mM dopant solution.

the 100 mM dopant solution. The linear magnetic field dependence is consistent with the ordinary Hall voltage behaviour (Fig. 2a). The 2D sheet carrier density, n_{2D}, is given by $n_{2D} = |(I_dB)/(e\Delta V_H)|$, where I_d is the drain current, e is the electric charge, B is the magnetic field strength and ΔV_H is the Hall voltage obtained after subtracting the offset Hall voltage at B = 0 T. The carrier mobility is given by $\mu = \sigma_{2D}/en_{2D}$, where σ_{2D} = 5.6 × 10^{-5} Ω^{-1} is the sheet conductance of the present device. The values of n_{2D} and μ were estimated to be 3.4 × 10^{13} cm^{-2} and 10 cm^2 V^{-1} s^{-1}, respectively. The present n_{2D} value is as high as the value of ~10^{13} cm^{-2} previously reported for MoS$_2$ doped with potassium or BV.[22,23] The high electron density also suggests that the Fermi level is located in the conduction band and that degenerate n-type doping is achieved by the crown ether complexes. Indeed, the temperature-dependent resistance of the doped MoS$_2$ indicates typical metallic behaviour, where the resistance decreases with decreasing temperature (Fig. 2b). These transport measurement results clearly indicate that effective electron doping was achieved by the crown ether complex-based coating process.

To understand the electronic states of monolayer MoS$_2$ with the K/benzo-18-crown-6 complex, we carried out first principles calculations. Fig. 3a shows the changes in the electron distribution as a result of the adsorption of the dopant. The region of increased electron density (indicated in blue) is distributed over the MoS$_2$ layer and the region of decreased electron density (indicated in orange) is distributed in the crown ether complex (Fig. 3b). Fig. 3c shows the electronic band structures. Monolayer MoS$_2$ has a direct bandgap of ~1.8 eV and its Fermi level is located in the middle of the bandgap. In contrast, the Fermi level of monolayer MoS$_2$ with the crown ether complex shifts to the conduction band. According to the density of states (Fig. 3d), the energy level of the highest occupied molecular orbital (HOMO) for the K/benzo-18-crown-6 complex (having K atom components) becomes higher than the conduction-band minimum of monolayer MoS$_2$. This arrangement of energy levels means that one electron is transferred from the complex to MoS$_2$ per unit cell. Assuming that the density of K/benzo-18-crown-6 complex on the MoS$_2$ layer is the same
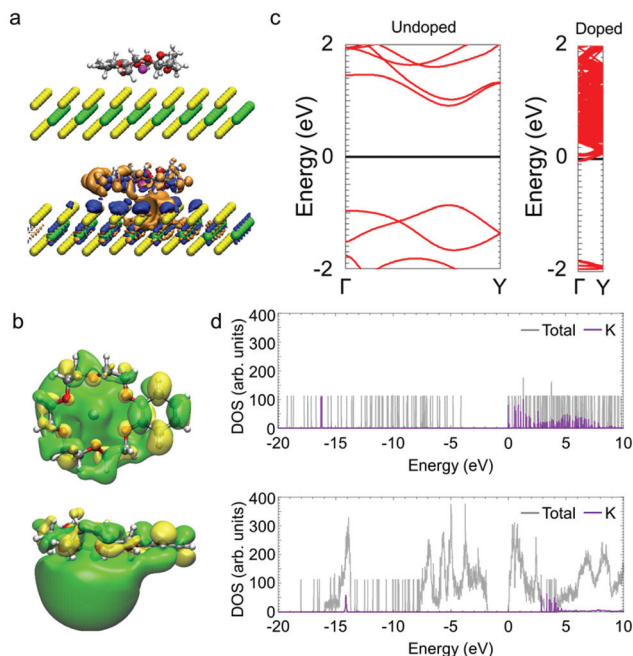
Fig. 3 (a) Optimized atomic structure of monolayer MoS$_2$ with the K/benzo-18-crown-6 complex and changes in the electron distribution induced by the adsorption of the dopant. Gray, red, white, purple, yellow and green spheres represent C, O, H, K, S and Mo atoms, respectively. The blue (orange) colour represents an increase (decrease) in the electron density. (b) Top and side views of the wave function of the HOMO for K/benzo-18-crown-6. The green and yellow colors indicate plus and minus contours, respectively. (c) Electronic band structures of undoped and doped monolayer MoS$_2$. (d) Total (gray) and K atom partial (purple) density of states (DOS) of (top) K/benzo-18-crown-6 and (bottom) monolayer MoS$_2$ with K/benzo-18-crown-6.

as that used in the model for calculations, the electron density of monolayer MoS$_2$ is estimated to increase to ~3×10^{13} cm^{-2}. This estimation is consistent with the carrier density obtained from the Hall effect measurement (Fig. 2a). These results also suggest that the doped electrons in MoS$_2$ are stabilized by the K/benzo-18-crown-6 complex after charge transfer from the OH$^-$ ions to MoS$_2$.

Next, we demonstrated the spatially controlled n-type doping of partially masked MoS$_2$ FETs. After the electrodes were deposited, an epoxy-based photoresist was coated, using a lithography process, only in the middle of the channel. The MoS$_2$ between the source/drain (S/D) contacts and the photoresist were then doped, whereas the channel masked by the photoresist remained undoped (Fig. 4a). Fig. 4b and Fig. S3† show the transfer and output curves of the device with the photoresist coating before and after the doping, respectively. The doped device clearly exhibits a higher on-current and a rapid increase in the current. Given the change in the channel area, the electron mobility increased from ~52 cm^2 V^{-1} s^{-1} to ~117 cm^2 V^{-1} s^{-1} as a result of the patterned doping.

The patterned n-type doping was also carried out by partial removal of KOH/benzo-18-crown-6. The dopant was removed by immersing the samples in a solvent such as water or butanol. After the devices were immersed in these solvents,
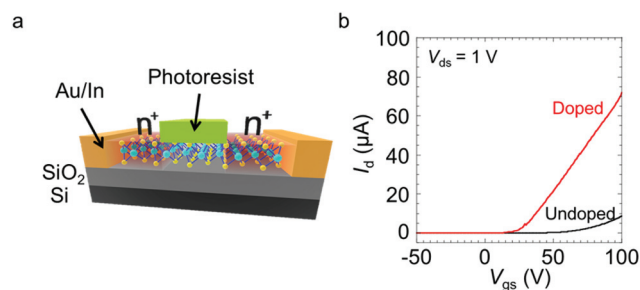

Fig. 4 (a) Schematic diagram of an n$^+$/i/n$^+$ patterned device with a photoresist coating. (b) Transfer curves of the device with the photoresist coating before and after the doping using 100 mM dopant solution.

the gate dependence of the washed MoS$_2$ exhibited n-type behaviour, with a high on/off current ratio, similar to the gate dependence of the undoped MoS$_2$ (Fig. S4a and b†). The patterned n-doping of the MoS$_2$ FETs was achieved *via* the reversible characteristics and the lithography process. After the doping, the photoresist was lithographically coated only close to the S/D electrodes. The dopant in the uncoated region was then removed by immersing the device in water for 1 min; the coated region remained in the doped state because of the protection afforded by the photoresist (Fig. S4c†). Fig. S4d† shows the transfer curves before and after the patterning. The on-current increased from ~6.6×10^{-7} to ~3.3×10^{-6} A. These results for both the partially doped devices, which are similar to the results for previously reported devices,[22,23,31] can be explained by a reduction in the contact resistance.

For discussion of the advantages of our doping method, the performance of TMDC-FET devices reported in the present work and in previous works are compared in Table S1.†[22–27] The present doping method achieved relatively high electron density (~3.4×10^{13} cm^{-2}) and air stability (~24 days) compared with the methods used to prepare devices in the previous studies. Rosa *et al.* have reported that poly(vinyl-alcohol) doping with Al$_2$O$_3$ encapsulation results in a device with high stability in air for 30 days.[26] Such oxide films may provide an approach to improve the stability of the present n-type doped TMDCs through passivation.

Conclusions

We have demonstrated the efficient electron doping of CVD-grown monolayer MoS$_2$ with high stability under ambient conditions using KOH/benzo-18-crown-6 as a dopant. The electron doping achieved a high electron density of 3.4×10^{13} cm^{-2}, and the doped MoS$_2$ exhibited excellent stability in air for ~1 month. First-principles calculations indicated that electrons were transferred from the K/benzo-18-crown-6 complex to the monolayer MoS$_2$. Patterned doping was also used to improve the contact resistance in MoS$_2$-based FETs. The present chemical doping strategy provides an effective method to control the electrical properties of TMDC materials for use in future device applications.

Experimental section

Sample preparation

MoS_2 monolayers were grown on SiO_2 (285 nm)/Si substrates via salt-assisted CVD.[41,42] The SiO_2/Si substrate was placed at the centre of a quartz tube, and MoO_2 powder (20–100 mg), KBr powder (5–11 mg) and sulphur flakes (2–3 g) were placed 1, 2–3 and 30 cm upstream from the tube centre, respectively. The quartz tube was then filled with N_2 gas at flow rates of 150–275 sccm. The temperatures of the substrate and powders were gradually increased to 740–800 °C using an electric furnace. After the set-point temperature was reached, the sulphur flakes were heated at about 180–200 °C for 15 min using a second electric furnace to supply sulphur vapor to the substrate. After the growth, the quartz tube was immediately cooled using an electric fan. The same reaction conditions were used to grow WS_2, except that WO_3 powder (10 mg) was used instead of MoO_2, the amount of KBr was decreased to 5 mg, and the N_2 gas flow rate was increased to 300 sccm.

Device fabrication

FET devices were fabricated by photolithography. MoS_2 films on SiO_2/Si substrates were spin-coated with an AZ P1350 photoresist (Merck Performance Materials), followed by an exposure/development process, resistive thermal evaporation of Au (20 nm)/In (5 nm) electrodes (ULVAC, EX-200) and a lift-off process in acetone. The devices were then annealed at 200 °C under vacuum (~10^{-4} Pa) for 30 min before the transport measurements. To prepare the four-terminal devices for Hall effect measurements, the devices were plasma-etched for 1 min using a Tergeo plasma cleaner (Pie Scientific) at 49 W under Ar and air. For the $n^+/i/n^+$ patterned doping, an SU-8 3005 photoresist (Kayaku Advanced Materials) was coated only in the middle of the channel using a lithography process. A similar $n^+/i/n^+$ patterned doping was achieved by combining an AZ P1350 photoresist coating applied only close to the S/D electrodes and water immersion after KOH/benzo-18-crown-6 doping.

Doping process and transport measurements

The carrier transport properties were measured using a probe station with voltage sources (KEITHLEY, 2614B) connected in the configuration. The doping process was performed by spin-coating butanol solution consisting of KOH/benzo-18-crown-6 (0.1–100 mM) onto the substrates. These chemicals were purchased from Wako Pure Chemical Industries (Japan) and Sigma-Aldrich (Japan) and were used as received without further purification. The Hall effect and the temperature dependence of the electrical resistance were measured with a physical property measurement system (PPMS, Quantum Design).

Raman and PL spectroscopy

The Raman and PL spectra of the samples were acquired at 532 nm excitation in a backscattering configuration using a microspectrometer (Renishaw, inVia).

Theoretical calculations

First-principles calculations of the undoped and doped monolayer MoS_2 were carried out using density functional theory (DFT), as implemented in the OpenMx package.[43] The generalized gradient approximation[44] with van der Waals correction[45,46] was used for the exchange–correlation function. The electron–ion interaction was described by norm-conserving pseudopotentials.[47,48] Pseudo-atomic orbitals (PAOs) centred on atomic sites were used as the basis function set.[49] The PAO basis functions were specified by C7.0-s2p2d1, H7.0-s2p1, O7.0-s2p2d1, K14.0-s4p3d2, M7.0-s3p2d2f1 and S7.0-s3p2d2f1. For example, C7.0-s2p2d1 indicates the PAOs of the carbon atom with a cutoff radius of 7.0 Bohr and with two s, two p, and one d components. The lattice constant of the monolayer MoS_2 was set to 3.16 Å.

Author contributions

Y.M. developed the concept and supervised the project. H.O. and M.K. fabricated the devices and performed the FET measurements. T.E. prepared the MoS_2 and WS_2 samples by CVD. Y. Nonoguchi prepared the KOH/benzo-18-crown6 solution. H.O. performed plasma etching together with K.Y., who provided technical assistance. J.P. and T.T measured the Hall effect and temperature dependence of the doped samples. M.O. performed the first-principles calculations. H.O. and T.I. carried out the patterned doping. H.O., M.K., Y. Nakanishi, H.E.L. and Y.M. prepared the figures and wrote the paper. All authors discussed the results and commented on the manuscript.

Conflicts of interest

There are no conflicts to declare.

Acknowledgements

Notes and references

1 D. Jariwala, V. K. Sangwan, L. J. Lauhon, T. J. Marks and M. C. Hersam, *ACS Nano*, 2014, **8**, 1102–1120.
2 H. Tian, M. L. Chin, S. Najmaei, Q. Guo, F. Xia, H. Wang and M. Dubey, *Nano Res.*, 2016, **9**, 1543–1560.
3 Z. Hu, Z. Wu, C. Han, J. He, Z. Ni and W. Chen, *Chem. Soc. Rev.*, 2018, **47**, 3100–3128.
4 L. Wang, L. Huang, W. C. Tan, X. Feng, L. Chen, X. Huang and K.-W. Ang, *Small Methods*, 2018, **2**, 1700294.

5   S. Ahmed and J. Yi, *Nano-Micro Lett.*, 2017, **9**, 50.

6   W. Liao, S. Zhao, F. Li, C. Wang, Y. Ge, H. Wang, S. Wang and H. Zhang, *Nanoscale Horiz.*, 2020, **5**, 787–807.

7   A. T. Hoang, K. Qu, X. Chen and J.-H. Ahn, *Nanoscale*, 2021, **13**, 615–633.

8   K. F. Mak, C. Lee, J. Hone, J. Shan and T. F. Heinz, *Phys. Rev. Lett.*, 2010, **105**, 136805.

9   B. Radisavljevic, A. Radenovic, J. Brivio, V. Giacometti and A. Kis, *Nat. Nanotechnol.*, 2011, **6**, 147–150.

10 H. C. P. Movva, A. Rai, S. Kang, K. Kim, B. Fallahazad, T. Taniguchi, K. Watanabe, E. Tutuc and S. K. Banerjee, *ACS Nano*, 2015, **9**, 10402–10410.

11 Y. Sun, D. Wang and Z. Shuai, *J. Phys. Chem. C*, 2016, **120**, 21866–21870.

12 A. Splendiani, L. Sun, Y. Zhang, T. Li, J. Kim, C.-Y. Chim, G. Galli and F. Wang, *Nano Lett.*, 2010, **10**, 1271–1275.

13 N. R. Pradhan, D. Rhodes, Q. Zhang, S. Talapatra, M. Terrones, P. M. Ajayan and L. Balicas, *Appl. Phys. Lett.*, 2013, **102**, 123105.

14 J. Suh, T.-E. Park, D.-Y. Lin, D. Fu, J. Park, H. J. Jung, Y. Chen, C. Ko, C. Jang, Y. Sun, R. Sinclair, J. Chang, S. Tongay and J. Wu, *Nano Lett.*, 2014, **14**, 6976–6982.

15 Y. Jin, Z. Zeng, Z. Xu, Y.-C. Lin, K. Bi, G. Shao, T. S. Hu, S. Wang, S. Li, K. Suenaga, H. Duan, Y. Feng and S. Liu, *Chem. Mater.*, 2019, **31**, 3534–3541.

16 S. Sasaki, Y. Kobayashi, Z. Liu, K. Suenaga, Y. Maniwa, Y. Miyauchi and Y. Miyata, *Appl. Phys. Express*, 2016, **9**, 071201.

17 H. Gao, J. Suh, M. C. Cao, A. Y. Joe, F. Mujid, K.-H. Lee, S. Xie, P. Poddar, J.-U. Lee, K. Kang, P. Kim, D. A. Muller and J. Park, *Nano Lett.*, 2020, **20**, 4095–4101.

18 Z. Qin, L. Loh, J. Wang, X. Xu, Q. Zhang, B. Haas, C. Alvarez, H. Okuno, J. Z. Yong, T. Schultz, N. Koch, J. Dan, S. J. Pennycook, D. Zeng, M. Bosman and G. Eda, *ACS Nano*, 2019, **13**, 10768–10775.

19 S.-S. Chee, C. Oh, M. Son, G.-C. Son, H. Jang, T. J. Yoo, S. Lee, W. Lee, J. Y. Hwang, H. Choi, B. H. Lee and M.-H. Ham, *Nanoscale*, 2017, **9**, 9333–9339.

20 M. Tosun, L. Chan, M. Amani, T. Roy, G. H. Ahn, P. Taheri, C. Carraro, J. W. Ager, R. Maboudian and A. Javey, *ACS Nano*, 2016, **10**, 6853–6860.

21 L. Yang, K. Majumdar, H. Liu, Y. Du, H. Wu, M. Hatzistergos, P. Y. Hung, R. Tieckelmann, W. Tsai, C. Hobbs and P. D. Ye, *Nano Lett.*, 2014, **14**, 6275–6280.

22 H. Fang, M. Tosun, G. Seol, T. C. Chang, K. Takei, J. Guo and A. Javey, *Nano Lett.*, 2013, **13**, 1991–1995.

23 D. Kiriya, M. Tosun, P. Zhao, J. S. Kang and A. Javey, *J. Am. Chem. Soc.*, 2014, **136**, 7853–7856.

24 S. Andleeb, A. K. Singh and J. Eom, *Sci. Technol. Adv. Mater.*, 2015, **16**, 035009.

25 A. Rai, A. Valsaraj, H. C. P. Movva, A. Roy, R. Ghosh, S. Sonde, S. Kang, J. Chang, T. Trivedi, R. Dey, S. Guchhait, S. Larentis, L. F. Register, E. Tutuc and S. K. Banerjee, *Nano Lett.*, 2015, **15**, 4329–4336.

26 C. J. Lockhart de la Rosa, A. Nourbakhsh, M. Heyne, I. Asselberghs, C. Huyghebaert, I. Radu, M. Heyns and S. De Gendt, *Nanoscale*, 2017, **9**, 258–265.

27 S. Zhang, H. M. Hill, K. Moudgil, C. A. Richter, A. R. Hight Walker, S. Barlow, S. R. Marder, C. A. Hacker and S. J. Pookpanratana, *Adv. Mater.*, 2018, **30**, 1802991.

28 X. Liu, D. Qu, J. Ryu, F. Ahmed, Z. Yang, D. Lee and W. J. Yoo, *Adv. Mater.*, 2016, **28**, 2345–2351.

29 H. G. Ji, P. Solís-Fernández, D. Yoshimura, M. Maruyama, T. Endo, Y. Miyata, S. Okada and H. Ago, *Adv. Mater.*, 2019, **31**, 1903613.

30 M. W. Iqbal, E. Elahi, A. Amin, S. Aftab, I. Aslam, G. Hussain and M. A. Shehzad, *Superlattices Microstruct.*, 2020, **147**, 106698.

31 H. Fang, S. Chuang, T. C. Chang, K. Takei, T. Takahashi and A. Javey, *Nano Lett.*, 2012, **12**, 3788–3792.

32 Y. Nonoguchi, M. Nakano, T. Murayama, H. Hagino, S. Hama, K. Miyazaki, R. Matsubara, M. Nakamura and T. Kawai, *Adv. Funct. Mater.*, 2016, **26**, 3021–3028.

33 G. W. Gokel, D. M. Goli, C. Minganti and L. Echegoyen, *J. Am. Chem. Soc.*, 1983, **105**, 6786–6788.

34 S. M. Sze, *Semiconductor Devices: Physics and Technology*, John Wiley & Sons, New York, 2nd edn, 2002.

35 A. M. van der Zande, P. Y. Huang, D. A. Chenet, T. C. Berkelbach, Y. You, G.-H. Lee, T. F. Heinz, D. R. Reichman, D. A. Muller and J. C. Hone, *Nat. Mater.*, 2013, **12**, 554–561.

36 C. Lee, H. Yan, L. E. Brus, T. F. Heinz, J. Hone and S. Ryu, *ACS Nano*, 2010, **4**, 2695–2700.

37 B. Chakraborty, A. Bera, D. V. S. Muthu, S. Bhowmick, U. V. Waghmare and A. K. Sood, *Phys. Rev. B: Condens. Matter Mater. Phys.*, 2012, **85**, 161403.

38 K. F. Mak, K. He, C. Lee, G. H. Lee, J. Hone, T. F. Heinz and J. Shan, *Nat. Mater.*, 2013, **12**, 207–211.

39 S. Mouri, Y. Miyauchi and K. Matsuda, *Nano Lett.*, 2013, **13**, 5944–5948.

40 Y. Kobayashi, S. Sasaki, S. Mori, H. Hibino, Z. Liu, K. Watanabe, T. Taniguchi, K. Suenaga, Y. Maniwa and Y. Miyata, *ACS Nano*, 2015, **9**, 4056–4063.

41 K. Kojima, H. E. Lim, Z. Liu, W. Zhang, T. Saito, Y. Nakanishi, T. Endo, Y. Kobayashi, K. Watanabe, T. Taniguchi, K. Matsuda, Y. Maniwa, Y. Miyauchi and Y. Miyata, *Nanoscale*, 2019, **11**, 12798–12803.

42 S. Li, S. Wang, D.-M. Tang, W. Zhao, H. Xu, L. Chu, Y. Bando, D. Golberg and G. Eda, *Appl. Mater. Today*, 2015, **1**, 60–66.

43 http://www.openmx-square.org/.

44 J. P. Perdew, K. Burke and M. Ernzerhof, *Phys. Rev. Lett.*, 1996, **77**, 3865.

45 S. Grimme, J. Antony, S. Ehrlich and H. Krieg, *J. Chem. Phys.*, 2010, **132**, 154104.

46 S. Grimme, S. Ehrlich and L. Goerigk, *J. Comput. Chem.*, 2011, **32**, 1456–1465.

47 N. Troullier and J. L. Martins, *Phys. Rev. B: Condens. Matter Mater. Phys.*, 1991, **43**, 1993.

48 L. Kleinman and D. Bylander, *Phys. Rev. Lett.*, 1982, **48**, 1425.

49 T. Ozaki, *Phys. Rev. B: Condens. Matter Mater. Phys.*, 2003, **67**, 155108.